

AN ANTI BACKLASH TWO-PART SHAFT COUPLING WITH INTERLOCKING ELASTICALLY AVERAGED TEETH

Mahadevan Balasubramaniam¹, Edmund Golaski¹, Seung-kil Son¹, Krishnan Sriram¹,
Alexander Slocum^{1*}

¹Department of Mechanical Engineering
Massachusetts Institute of Technology
Cambridge, MA 02139

Abstract

A new family of compliant and self-locking tapered torsional couplings have been developed as an alternate to spline-type couplings. The couplings use designed compliance to ensure constant contact between mating beam-like teeth. The tip of one tooth is larger, but tapered, so that when it mates at the base of the opposed tooth, it deflects radially. The taper is self-locking to prevent radial deflection under torsional load. This eliminates backlash between parts while maintaining a relatively high torsional stiffness. The large number of mating teeth elastically average errors in the teeth.

Keywords: Torsional couplings, Elastic averaging

1.0 INTRODUCTION

There are many types of torsional couplings for blind mating including spline-type couplings such as splines, oldham and spiders couplings[8]. In torsional spline-type couplings, backlash between projecting elements leads to wear of the coupling and noise; eventually causing the spline to fail. The goal of this project was to develop a new coupling that eliminated backlash while maintaining the simple assembly associated with spline type couplings.

With respect to the design of zero backlash couplings, there are two schools of thought: kinematic and elastically averaged designs. The former are well documented [1, 2], but unless complex flexures are added [3], they cannot accommodate dynamic misalignment between components. Elastically averaged systems achieve repeatability or prevent backlash by having a continuum of points in contact, either by flexing of a material (e.g., a flexural coupling such as a Helical™ coupling) or preloading of many points such that the error in any one subcomponent is averaged out by elastic deformation (e.g., a curvic coupling or preloaded bearings in a universal joint) [4, 5].

The dilemma, however, is that flexural couplings require a means to clamp the coupling to a shaft, preventing blind assembly. In addition, preloading a coupling's elements to achieve elastic averaging involves large forces or complexity that also precludes blind assembly. The new family of couplings presented here combines blind assembly with elastic averaging and self-locking tapers to prevent slip between coupling elements.

* Corresponding author

2.0 SPLINE ALTERNATIVES

There are many alternatives to spline couplings for transmitting torsional loads while providing modest shaft misalignment capability. Elastomeric and flexural couplings [6,7] have greater compliance between the driving shaft and the driven shaft, as well as more parallel misalignment. The soft materials reduce noise and fatigue, but they preclude accurate rotational motion. Elastomeric couplings are generally divided into compressive and shear couplings, depending on the interaction mode of the driving and driven shafts. In a compressive coupling, parts of the driving shaft push on parts of the driven shaft. Elastomeric material is placed between the interacting faces and absorbs some of the torsional energy through compression. In a shear coupling, both the driving and driven shafts are connected only to the elastomeric material, placing the elastomer in shear during torque transmission. Elastomers are both stiffer and stronger in compression than shear, so compressive couplings are typically torsionally stiffer and can carry a higher torque load than can shear couplings. Thus, compressive couplings are a better choice in applications requiring some positioning accuracy or high torque loads, while shear couplings are well suited to damping out torsional vibrations. Shear couplings are also superior in applications with high angular or axial misalignment.

Hybrid couplings combine features of metallic and elastomeric couplings. Commonly, they have a higher torsional stiffness, like a metallic coupling, but allow considerable angular and axial misalignment, as would an elastomeric coupling. Couplings with this type of “hybrid” behavior are sometimes made of composite materials that perform better in harsh chemical environments than would elastomers. However, there is still the problem of how to achieve blind assembly.

3.0 CONCEPT DEVELOPMENT

3.1. Early Concepts

Numerous concepts for a backlash-free blind-mating coupling were evaluated before the concept discussed in detail here was selected. Six were selected as the most promising as shown in Figure 1 a-f. Table 1 summarizes the dominant physics, risks, and benefits of each concept. The first was a kinematic coupling between shafts (Fig. 1a); this would guarantee constant contact between the shafts, preventing backlash, and would also allow simple blind assembly. However, it would not accommodate misalignment. A contrasting option was a torque finger connection (Fig. 1b); many elastic fingers on the end of each shaft mesh together to transmit torque. This concept uses elastic averaging to average out errors in the fingers’ geometry. This ensures that for modest misalignments or manufacturing errors, mating fingers are always in contact, preventing backlash. Torque fingers would allow looser manufacturing tolerances and easy assembly, but the torque capacity might not be as high as with other alternatives.

Two concepts involving compliance were also considered. The first was a compliant spline (Fig. 1c). Leaf spring-like features would be incorporated into the shape of the spline keys (not shown) or keyways (shown) and would be preloaded when the keys were inserted into the key ways. This preload guarantees constant contact, eliminating backlash. This concept would allow one-step assembly, but the leaf spring features would make the coupling more complex to manufacture than a simple spline.

Another alternative used elastomeric inserts (Fig 1d) in a spline connection similar to the current one. Like

Table 1: Characteristics of various coupling alternatives

Concept	Physics of Operation	Major benefits	Risks/Drawbacks
Kinematic Coupling	6 point contact (Figure 1a)	Drop-in assembly	Cannot accommodate mis-alignment
Torque Fingers	Elastic averaging of many meshing fingers (Figure 1b)	Loose manufacturing tolerances Easy assembly	Low Torque capacity
Compliant spline	Compliance built into spline keys or keyways (Figure 1c)	Reduce backlash Simple Assembly	Manufacturing complexity
Elastomeric Inserts	Insert/Inject elastomer between spline keys & keyways (Figure 1d)	Evolutionary idea High damping	Messy, complex reassembly process
Wedge spline	Sliding wedges expand key to fill keyway (Figure 1e)	Zero backlash High stiffness	Complex parts Adjustment required
Friction coupling	Conical friction surfaces Axial force supplied by bolt (Figure 1f)	High damping	Wear Angular misalignment capability Low Torque Capacity
Self adjusting compliant couplings	Fingers which deflect to accommodate manufacturing variations (Figure 1g)	Drop in assembly No backlash High Stiffness Good damping	Modest misalignment capability

the elastomeric couplings discussed above, these inserts would not eliminate backlash, but they would absorb energy and eliminate rattle. The insert could be a resin injected in the form of a liquid under pressure and allowed to cure. However, such inserts could add considerable complexity to the assembly process and for rework should the coupling require disassembly.

A further idea (Fig 1e) also altered the basic spline concept to ensure constant contact, splitting each spline key into two wedges that can slide against each other. As they slide, the effective width of the key changes. Adding an appropriate preload will maintain a key width sufficient for constant contact.

The last alternative concept considered was a friction coupling (Fig 1f). Two shafts would have mating conically shaped ends with an elastomer bonded to their surfaces. An axial bolt would be tightened to create the desired normal force between the two faces, with frictional force being proportional to the normal force. This concept eliminates backlash, but does require the extra assembly step of bolt tightening. Such a design would have little allowance for misalignment.

Figure 1g evolved by combining the positive features of the other couplings along with the concept of elastic averaging and self-locking tapers; and it is the basis of the new coupling concept.

3.2. New Coupling Concept

The new coupling uses the principle of matched compliance between radially tapered beams and consists of two pieces, either symmetrical or asymmetrical, engaging through fingers which behave as cantilever

beams. The ends of the fingers from one piece engage the roots of the fingers from the other, and vice versa. The effect is to have two sets of rigid-compliant engagement beams. This rigid-compliant engagement provides a tight, preloaded coupling between parts that are relatively insensitive to manufacturing variations. Unlike tapered tooth couplings, the transmission of torque does not result in a net axial force. While the overall coupling may be short relative to its diameter, each beam will have a slender aspect ratio, such that one end is compliant, whereas the other is relatively rigid.

We define the *working direction* as the direction in which net force is transmitted by the teeth. It is the direction of instantaneous velocity for any given particle in the coupling, and lies in a plane normal to the axis of the coupling.

We define the *adjustment direction* as the direction in which the elements of the coupling flex to accommodate manufacturing variation. In Figure 2, the working direction and adjustment direction are indicated for an example location on the coupling cross section, when the torque is applied along the z direction. In one concept variant, the adjustment direction is parallel to the working direction (Figure 3,5). In other implementations, it is perpendicular to the working direction (Figure 4).

3.3. Concept Variant: Circumferential Adjustment Compliance

The simplest embodiment provides circumferential compliance between the teeth to adjust for coupling tooth errors. Examples of this can be seen in Figures 3 and 5.

In this concept, the stiffness of the coupling for small deflections is reduced. The same mechanism which permits the coupling to adjust permits the fingers to deflect under load. For larger deflections, the adjustment mechanism may "bottom out", leading to solid contact. For large torques, this effect may be felt as backlash. It should be noted that the adjustment compliances for all varieties of coupling in the family are in parallel with each other, with respect to torsional stiffness. That each coupling has many fingers lessens the consequences of the adjustment and working directions being parallel.

3.4. Concept Variant: Radial Adjustment Compliance

In this concept, the working surfaces of the coupling are radially tapered by an angle α . During installation, variations in the width of the fingers in the working direction are accommodated by the finger flexing in the radial direction. The angle formed couples the width of the finger to its radial distance from the central axis. This permits looser manufacturing tolerances - if the fit is tighter than expected, one finger deflects inward and the other finger outward. The angle ensures good contact between the pieces. Generous chamfers at the ends of the fingers make alignment easier, and reduce the starting force for assembly. A simple example of this idea can be seen in Figure 4. In order to keep the pre-load forces to a small value, we need to have lesser stiffness along the adjustment direction. However, care should be taken not to reduce the tangential stiffness so that the coupling does not twist too much under torque loads. If we have a large diameter as well as a hollow inside, we can achieve high tangential stiffness as well as low radial stiffness. Note that for a torsional coupling, the perpendicular adjustment direction is equivalent to the radial direction.

If the angle is small enough relative to the coefficient of static friction [Equation 21], it can be shown that the device becomes self-locking, which is a key feature of this concept. Force is transmitted in the working direction without any deflection in the adjustment direction. This increases the torsional stiffness of the coupling.

3.5. Concept Embodiment: Moment Carrying

If the overall coupling is long relative to its diameter, it will be able to support bending moments. In order

to achieve matched compliance, each finger should have an aspect ratio of approximately 10 to 1, thus for a small number of fingers, the overall coupling aspect ratio is on the order of 3 or 4 to 1. Four-finger moment-carrying couplings are shown in Figures 3-5.

3.6. Concept Embodiment: Non-Moment Carrying

This embodiment (Figures 6,7) is intended for applications in which length is short, and moments need not (or should not) be resisted. Once the engagement length of the coupling is determined, the fingers can be sized to have the required stiffness profile. This yields the required width of each finger, and a fully populated coupling then contains as many fingers as fit around its circumference.

3.7. Design Issues

We have used the terms "relatively stiff" and "relatively compliant" to mean that the beam, or finger, should be much more compliant at the end than at the root, perhaps one order of magnitude more compliant. From beam theory, the stiffness of a cantilever beam k is related to the distance x from the free end as $k \propto (1/x^3)$. As we go twice the distance towards the free end from a particular point, the stiffness nearly drops by an order of magnitude. We thus obtain a design equation for the length of the fingers based on the relative stiffness desired. In addition, rigid couplings will have damping at each mechanical contact. In our proposed coupling concept (Figure 6,7), damping is introduced by friction in the joints of several mating finger pairs. Quantifying the effect of damping due to several mating fingers in our coupling is a topic for further investigation.

Current belief holds that two-point contact between each pair of beams is essential to the success of the coupling. Each beam should contact the mating part only near the free end and near the root. (Two-zone rather than two-point contact would be a more accurate term in the 3D case.) Contact in the middle of the beam does not provide the desired matched compliance and has no moment carrying capacity.

The radius of contact (from the axis of rotation) in the coupling is important, since contact forces decrease with increasing radius of contact. Although part radius is a function of the torque to be transmitted and the materials available, steps can be taken to ensure that for a given part radius, the radius of contact is maximized.

4.0 SKETCH MODELS

Three wood models of coupling concepts were constructed to form physical "sketch models" that could be handled as a means to quickly physically evaluate concepts. If the coupling concept was robust, it should be able to accommodate the errors associated with novice woodworking. The first was of the basic matched-compliance concept, as seen in Figure 3. The second and third addressed compliance to allow for manufacturing errors. In the second, shown in Figure 5, adjustment is parallel to the working direction, and consists of a new male component for the old female component. The third uses beveled fingers which adjust normally to the working direction, requiring both a new male and female component. This model is shown in Figure 4.

All of the models are of glued-assembly construction to minimize the complexity of machining required. Segments of 25 mm (1" nominal) square stock (30 cm long for the fingers, and 10 cm long for core support) were finished and glued together in a grid to form the male and female components. Precision was achieved by using the same machine settings wherever possible; thus, the square stock pieces may not have been exactly 25 mm square, but they were square, and all the same. This symmetry greatly simplified the

tolerancing and measurement requirements. Due to quirks of the fabrication of the models, each model had a preferred assembly orientation.

The radial adjustment compliance model was given a generous chamfer to ease assembly. Without the chamfer the coupling halves required a great deal of force to assemble. With the chamfer, it assembled quite easily, even in the three non-preferred orientations. The effect of the chamfer on ease of assembly cannot be overstated; the tolerance for variation in a chamfered, perpendicular adjusting wooden model with non-trivial variations demonstrates the robustness of the matched-compliance principle.

All three models demonstrated excellent empirical torsional stiffness, as tested by twisting by hand. The parallel versions exhibited some minor creaking, suggesting flexing on a very small scale. The radial adjustment compliance, especially when assembled in a non-preferred direction, felt exceptionally stiff.

Physical models of the non-moment carrying versions of the coupling were produced by 3D printing. Circumferential and radial adjustment compliance proof-of-concept models are shown in Figure 6 and Figure 7, respectively. As expected, these models exhibited good torsional stiffness but were unable to resist large off-axis moment loads; thus demonstrating their coupling capability.

5.0 ANALYTICAL MODELS

A first-order analytical model was created to determine the torsional stiffness of a finger pair. The analysis is extended to determine the torsional stiffness of the couplings with parallel and perpendicular adjustment. Following this, a first-order model was created to determine the bending moment stiffness of the finger pair. The analysis is extended to determine the bending moment stiffness of the couplings with parallel and perpendicular adjustment.

5.1. Torsional stiffness

5.1.1. Stiffness of a finger pair

Consider a cantilever with the following dimension: length l , width b and height h . The stiffness of the cantilever at any section can be determined from the first-order analysis of a cantilever subjected to a concentrated load.

Therefore the spring constant at any section of the cantilever can be written as

$$K_x = \frac{3EI}{x^3} \quad (1)$$

Figure 8 shows the modeling of a pair of contacting fingers as rigid surfaces connected by compliant springs. The springs correspond to the compliance of the finger at the respective location. The spring constant at the base of the cantilever will be an order of magnitude higher than that at the tip. Therefore, the two springs can be replaced by a single spring with a spring constant corresponding to the stiffness of the free end of the cantilever.

The torsional constant of a finger pair can be found by representing the displacement δ at position x in terms of the radius of the coupling and the angular deflection; therefore,

$$\delta = r\delta\theta \quad (2)$$

the torsional spring constant is given by

$$K_t = K_x r_{mean}^2 \quad (3)$$

where r_{mean} is the mean radius of the coupling. Since there are 2 springs in parallel in a finger-pair

$$K_{t, fingerpair} = 2K_t \quad (4)$$

5.1.2. Torsional Stiffness of Circumferential Adjustment Compliance Couplings

Given mean radius of coupling r_{mean} , thickness of coupling δ_r , number of fingers on each coupling half n , width of a finger w , and gap to width ratio gw_{ratio} ,

we can relate the radius, width, and number of fingers (Figure 9) as

$$w = \frac{2\pi r_{mean}}{2n} \quad (5)$$

The effective width of the finger taking the gap width ratio is given by

$$w_{effective} = \frac{w(1 - gw_{ratio})}{2} \quad (6)$$

Therefore

$$I = \frac{\Delta r (w(1 - gw_{ratio}))^3}{96} \quad (7)$$

$$K_{t, fingerpair} = \frac{2(3)E\Delta r (w(1 - gw_{ratio}))^3 r_m^2}{96L^3} \quad (8)$$

Since the stiffnesses of the finger pairs are in parallel, the torsional constant of the entire coupling is obtained by adding the stiffnesses of its finger pairs. Therefore

$$K_{t, total} = nK_{t, fingerpair} \quad (9)$$

$$K_{t, total} = \frac{nE\Delta r (w(1 - gw_{ratio}))^3 r_m^2}{16L^3} \quad (10)$$

From this, we observe that for a given $\frac{l}{w}$, K_{total} increases linearly with respect to n , and for a given n , K_{total} decreases with the cube of $\frac{l}{w}$ as shown in Figure 10.

5.1.3. Torsional Stiffness of Radial Adjustment Compliance Couplings

In this coupling, the entire width of the finger contributes to the torsional stiffness. Therefore the stiffness can be obtained from the previous analysis by setting $w_{effective} = w$.

From this, we again observe that for a given $\frac{l}{w}$, K_{total} increases linearly with respect to n , and for a given n , K_{total} decreases cubically with $\frac{l}{w}$ as shown in Figure 11.

5.2. Bending moment stiffness

For a cantilever subjected to a moment, M ; The mean angular deflection at the free end is given by

$$\theta_{mean} = \frac{Ml}{2EI} \quad (11)$$

where l is the length of the cantilever, E is the modulus of elasticity, and I is the moment of inertia of the beam cross-section. Therefore

$$K_b = \frac{2EI}{l} \quad (12)$$

Since there are two fingers in a finger pair,

$$K_{b, fingerpair} = \frac{4EI}{l} \quad (13)$$

A finger can be subjected to bending in two directions, namely the radial direction, e_r and the tangential direction, e_θ . The bending stiffness in a direction can be obtained by using the appropriate area moment. Therefore, use I_θ for bending along the e_θ and I_r for bending along e_r .

5.2.1. Bending Stiffness of couplings

The bending stiffness of the coupling is determined by summing the contribution of its individual fingers. The amount of contribution is determined by

- Geometrical constraint on the finger
- Location of the finger pair with respect to the moment axis

Cosine effect: The bending of the fingers along e_θ can resist moments along e_r direction. Therefore the contribution of the finger depends on the projection of e_r along the external moment axis vector, \hat{i} . The magnitude of the projection is given by $|\vec{e}_r \cdot \hat{i}|$. If θ represents the spatial location of the finger-pair with respect to the \hat{i} , then the magnitude of the projection reduces to $|\cos(\theta)|$.

Sine effect: Similarly, the bending of the fingers along e_r can resist moments along e_θ direction. Therefore the contribution of the finger depends on the projection of e_θ along the external moment axis vector, \hat{i} . The magnitude of the projection is given by $|\vec{e}_\theta \cdot \hat{i}|$. If θ represents the spatial location of the finger-pair with respect to the \hat{i} , then the magnitude of the projection reduces to $|\sin(\theta)|$.

5.2.2. Bending Stiffness of Circumferential Adjustment Compliance Couplings

Given r_{mean} , mean radius of coupling, δ_c , thickness of coupling, n , number of fingers on each coupling half,

w , width of a finger, and gw_{ratio} , gap to width ratio, we can relate the radius, width and the number of fingers as

$$w = \frac{2\pi r_{mean}}{2n} \quad (14)$$

The effective width of the finger taking the gap width ratio is given by

$$w_{effective} = \frac{w(1 - gw_{ratio})}{2} \quad (15)$$

Therefore, the moduli governing the stiffness of a finger bending in the radial and tangential directional directions of the coupling are respectively:

$$I_r = \frac{\Delta r (w(1 - gw_{ratio}))^3}{96} \quad (16)$$

$$I_\theta = \frac{\Delta r^3 w(1 - gw_{ratio})}{12} \quad (17)$$

From the geometry of the fingers, there is no locking between the fingers to prevent the slip along e_r . Therefore, only the cosine effect is present when determining the contribution of the individual finger-pairs to the entire coupling.

$$K_{t, bending} = \frac{4EI_r}{l} (1 + |\cos(\theta)| + |\cos(2\theta)| + \dots + |\cos((n-1)\theta)|) \quad (18)$$

For a given $\frac{w}{l}$, the variation of $K_{\{t, bending\}}$ with n and for a given n , the variation of $K_{\{t, bending\}}$ with respect to $\frac{w}{l}$ are shown in Figure 12.

The first order mathematical model was analyzed to determine the effect of the number of fingers on the bending stiffness of the coupling. On plotting $K_{t, bending}$ versus the number of fingers, a kink was observed. We were able to explain the kinks mathematically from the equations. For the case when there were three fingers, the angle between the fingers is 120° . The sum of $1 + |\cos(120^\circ)| + |\cos(2*120^\circ)|$ is 2. While this sum for the 4 finger case, $1 + |\cos(90^\circ)| + |\cos(180^\circ)| + |\cos(270^\circ)|$ is also 2. As a result, in Figure 12 we observe a kink in the graph at $n=4$.

5.2.3. Bending Stiffness of Radial Adjustment Compliance Couplings

Here, the entire width of the finger contributes to the bending stiffness. The area moment can be computed using the formula given in the parallel case by setting $w_{effective} = w$. Since the geometry of the fingers ensures that locking occurs, a finger-pair can resist moments along both e_r and e_θ . Therefore, both sine and cosine effect is present when evaluating the contribution of the individual finger pairs to the overall

coupling:

$$K_{t, bending} = \frac{4EI_r}{l}(1 + |\cos(\theta)| + |\cos(2\theta)| + \dots + |\cos((n-1)\theta)|) \\ + \frac{4EI_\theta}{l}(1 + |\sin(\theta)| + |\sin(2\theta)| + \dots + |\sin((n-1)\theta)|)$$

For a given $\frac{l}{w}$, the variation of $K_{\{t, bending\}}$ with n and for a given n , the variation of $K_{\{t, bending\}}$ with respect to $\frac{l}{w}$ are shown in Figure 13 where kinks occur as explained in the previous section.

6.0 SELF LOCKING AND FINGER GEOMETRY

This section describes the mechanics of frictional interlocking between the coupling fingers. The idea is extended to determine the angle of the sloping faces of the finger required for self-locking. During our experimental phase, our first design displayed relative slip between the fingers of the male and the female elements. As explained in Section 3.4, relative slip between fingers is detrimental to the torsional stiffness of the coupling. The design was analyzed and the reason for the slip was identified and corrected in the next design.

6.1. The Self Locking Effect

Figure 14 shows a block lying on a flat surface which is being acted upon by an external force F at an angle β with the surface. If μ_s is the coefficient of static friction between the block and the surface, then, neglecting gravity, the block will remain stationary as long as the following conditions are valid.

$$N = F \sin(\beta) \tag{19}$$

$$\mu_s N > F \cos(\beta) \tag{20}$$

Therefore, a simple condition for self locking is

$$|\tan(\beta)| \mu_s > 1 \tag{21}$$

6.2. Side Face Inclination of the Finger

Given the tangential force at the mean radius of the coupling is the external force acting on the inclined surface, as shown in Figure 14, let ϕ be the angle made by the side face of the fingers with the radial line. Using the self-locking result of Equation 21, we can determine an inequality relating ϕ and μ_s .

$$\phi = \frac{\pi}{2} - \beta \tag{22}$$

Therefore

$$\left| \tan\left(\frac{\pi}{2} - \phi\right) \right| \mu_s > 1 \tag{23}$$

$$\mu_s > |\tan(\phi)| \tag{24}$$

For a given μ_s , the maximum value of the inclination angle is given by

$$\phi < \tan^{-1}(\mu_s) \quad (25)$$

7.0 FINITE ELEMENT MODELS

Finite element models were created and evaluated using ProENGINEER™ and ProMECHANICA™. Torsional loads were applied as point loads. Note that ProMECHANICA™ automatically distributes a point load over a small circular area; this area is small relative to the size of the components, and does not significantly change our results.

Initial models were done on single fingers or finger pairs to save computation time. After these models demonstrated the feasibility of the idea, models of entire couplings were constructed and analyzed. Sample results are shown in Figures 15 and 16. Figure 15 is a plot of displacement magnitude in an aluminum model of the perpendicular adjustment moment carrying variation; displacement is expressed in units of milli-inches. Figure 16 shows strain energy for the 3D printed perpendicular adjustment non-moment carrying variation. These figures show good strain and stress distribution indicating a robust design.

8.0 TESTING AND RESULTS

Physical models were tested to validate analytical and finite element models of torsional stiffness. Figure 17 shows a test fixture that was constructed to permit the testing of 3D-printed couplings, as well as an aluminum model fabricated specifically for the tests.

Except where noted, all structural components were aluminum, and all fasteners and bearings were steel. The base of the test fixture was a 25mm (1" nominal) thick plate, resting on four feet. To this plate were bolted two bearing blocks and a coupling mounting block. The bearing blocks were mounted approximately 13 cm (5") apart, and supported a shaft with 25.4 mm (1") bore ball bearings. Into one end of a shaft was threaded a 1/2-20 steel hex-head bolt for torque application. The other end of the shaft featured a rectangular tongue, which meshed with a slot on the end of the coupling to be tested.

The tongue-slot design is analogous to half of an Oldham coupling. This arrangement allowed for torque to be applied to the test artifact with a simple socket-type torque-wrench, while isolating the artifact from forces other than arising out of pure torsion.

Deflection was measured by radially attaching a 6.35 mm threaded rod into each artifact. A dial indicator was used to measure deflection of the rod at a given distance (correcting for cosine error) as torque was applied with the wrench. The torsional stiffness of any components between the rod and the wrench were irrelevant, as torque is constant through the fixture.

The results of the testing are shown in Figures 18 and 19. In each case, deflection varies linearly with torque, as expected. The aluminum model (moment carrying) proved to be stiffer than the simple first order theory predicted. The torsional stiffness of the aluminum coupling is 1.5 N-m/milli-radian.

Table 2: Torsional deformation values for 3D printed coupling models

Coupling type	Moment carrying radial adjustment compliance model	Non-moment carrying circumferential adjustment compliance model
Applied torque	20 Nm	7 Nm
Experimental deflection value	21.6 milli-radians	19.6 milli-radians
FEA deflection value	14.5 milli-radians	13.6 milli-radians
Analytical deflection value	16.4 milli-radians	16.2 milli-radians

To compare it with a conventional spline coupling, we performed FEA analysis on a conventional spline coupling made of Al 6061, assuming single-tooth contact over a length of 50mm. The stiffness in this case was found to be 5.0 N-m/milli-radian. We have assumed line contact for the FEA analysis, but in reality, the spline teeth are likely to have point contact only and the stiffness value for the spline coupling would be lower. Thus, we observe that the proposed coupling has torsional stiffness comparable to conventional spline couplings with nearly same dimensions.

The 3D printed parts (non-moment carrying), on the other hand, proved more compliant than predicted. Here, several factors come into play. First, the parts are not solid, but composed of layers of a deposited polymer. In the parallel coupling, the core of each finger is of lower density. The anisotropic character of the 3-D printed parts explains some of the discrepancy. Further, the modulus of elasticity of the polymer and the coefficient of friction were not known precisely, leading to further disagreement between theory and experiment. Still, the general agreement indicates that an analytical model can be an aid in the design of this type of coupling. Experimental values are compared with analytical and finite element values in Table 2.

The first 3D printed perpendicular-type coupling exhibited relative slip between the fingers, indicating that self-locking was not occurring. Figure 19(b) shows the results for a 3D printed coupling re-designed to ensure self-locking. The new coupling was 1.25 times the diameter of the old coupling. Since torsional stiffness is proportional to the stiffness of the finger times the radius squared, the size of the new coupling alone should approximately double the stiffness. Recall the proportional relationship between the number of fingers and the stiffness shown in Figure 11. The smaller coupling has 9 teeth, whereas the larger coupling has 15 teeth. Thus, the increase in stiffness due to the number of teeth is approximately 1.7. The expected net stiffness ratio between the larger and smaller coupling is then 3.3. Comparison of the deflections from Figure 19(a) and Figure 19(b) shows approximately 4 times the stiffness, with the additional increase probably due to the self-locking effects.

9.0 CONCLUSIONS

This new family of couplings, inspired by backlash in spline-type couplings, uses the principle of interlocking fingers with designed compliance and self-locking taper angles to ensure constant contact of mating parts and thus eliminate backlash. The couplings are self-adjusting upon assembly; adjustment may be either circumferential or radial. Given a relatively constant aspect ratio of tooth length to width, the number of teeth will determine whether or not the coupling can carry off-axis moment loads. The self-locking phenomenon has been shown to contribute to torsional stiffness.

Analytical models of the coupling designs agreed with experimental results for stiffness to within 20 percent. Our finite element models were within 15 percent of measured values. Thus, the models and design metrics are useful for designing the couplings.

Further work is planned within this family of couplings. We will pursue a more accurate bending model and also plan to investigate the possibility of a radial version of this new type of coupling. The concept of the radial version of this coupling is as shown in Figure 20. In addition it may be possible to create these types of features on silicon wafer, so that the accuracy in assembly of MEMS devices can be increased.

10.0 ACKNOWLEDGMENTS

This work started as a team project for the course 2.75 — Precision Machine Design, taught by Prof. Alex Slocum at MIT. Heather Dunn was part of the team during the course project and participated in the initial concept development. We appreciate her valuable initial contribution to this project.

We would like to thank Dr. Zafar Shaikh and the Ford Motor Company for the 3D printed parts. We would also like to acknowledge the contribution of Ken Stone of the MIT Hobby Shop and Gerry Wentworth, Mark Belanger, and Bob Kane of the Laboratory for Manufacturing and Productivity machine shop for their assistance with the fabrication of the coupling models, respectively.

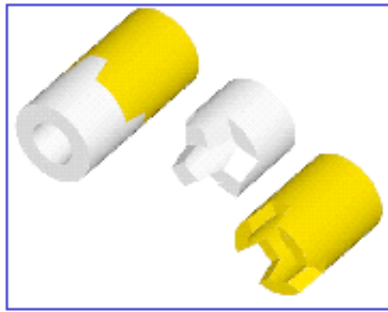
11.0 REFERENCES

1. Slocum, A. H. , “Design of Three-Groove Kinematic Couplings”, Precision Eng., Vol. 14, No. 2, April 1992, pp 67-76.
2. US Patent #6,065,898, L. Hale, “Three Tooth Kinematic Coupling”, May 2000
3. US Patent #5,678,944, A. Slocum, D. Braunstein, L. Muller, “Flexural Kinematic Couplings”, October 1997
4. Evans, C, Precision Engineering: An Evolutionary View, Cranfield Press, Bedford MK43 0AL, England
5. Slocum, A. H., Precision Machine Design, Prentice Hall, Englewood Cliffs N.J., Copyright 1992.
6. McCullough, M., “Selecting Elastomeric Couplings”, Plant Engineering, 9 January 1995.
7. McCullough, M., “Sorting Out Flexible Couplings”, Machine Design. 28 September 1995: 105.
8. Shigley, J. E., “Standard Handbook of Machine Design”, 2nd edition, McGraw-Hill Higher Education, ISBN: 0070569584.
9. Hale, L. C., and Slocum, A. H., “Design of anti-backlash transmissions for precision position control systems”, Precision Eng., 16(4), Oct 1994, pp 244-257.

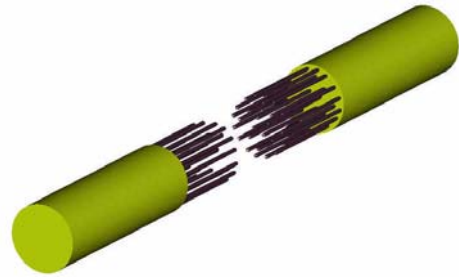
12.0 APPENDIX - NOMENCLATURE

μ_s	Coefficient of static friction
β	Angle made by applied force with the horizontal
δ	Deflection of the beam along the circumference
$\delta\theta$	Torsional deflection of the beam
Δr	Thickness of the coupling
ϕ	Angle of inclination of a surface
θ_{mean}	Mean angular deflection of the free end of the beam

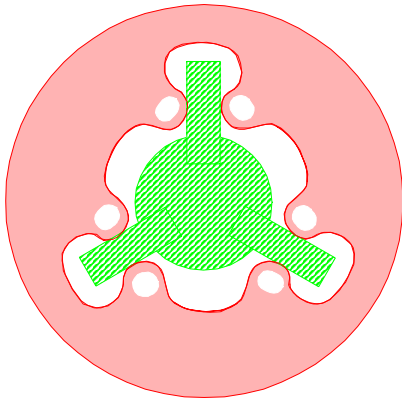
θ	Angular displacement variable
b	Width of a cantilever beam
\mathbf{e}_r	Unit vector in the radial direction
\mathbf{e}_θ	Unit vector in the tangential direction
$g_{w_{ratio}}$	Gap to width ratio in our coupling
h	Height of a cantilever beam
k	Stiffness of a beam
l	Length of a cantilever beam
n	Number of finger pairs
r	Radial distance from the axis
r_{mean}, r_m	Mean radius of the coupling
w	Width of a finger of the coupling
$w_{effective}$	Effective width of a finger based on gap-width ratio
x	Distance variable along an axis
E	Modulus of elasticity
F	Force
I	Moment of inertia of a beam about the neutral axis
I_θ	Moment of inertia of a finger about the neutral axis along the tangential direction
I_r	Moment of inertia of a finger about the neutral axis along the radial direction
K_b	Bending stiffness
K_t	Torsional stiffness
$K_{t-fingerpair}$	Torsional stiffness for a pair of fingers in contact
$K_{t-total}, K_{total}$	Torsional stiffness for the entire coupling
$K_{t-bending}$	Total bending stiffness of the entire coupling
K_x	Stiffness constant as a function of distance x along the beam
L	Length of a finger in the coupling
M	Moment
N	Normal force of reaction



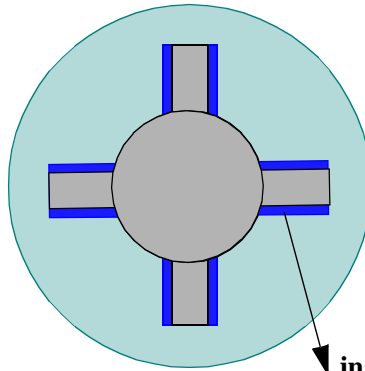
(a) Kinematic coupling



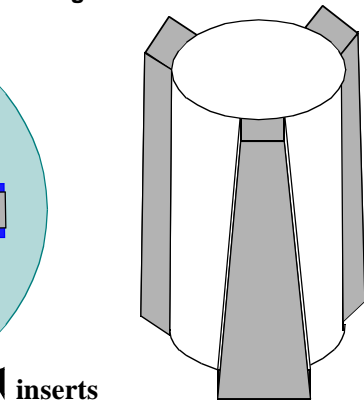
(b) Torque Fingers



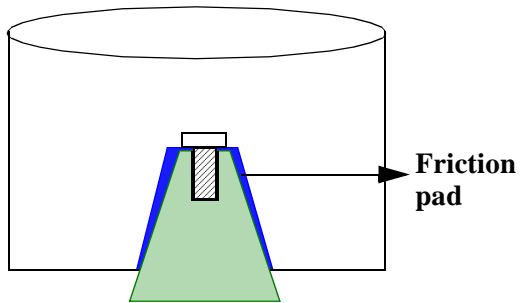
(c) Compliant splines



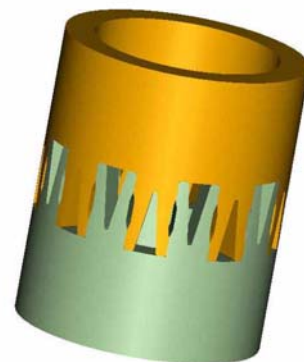
(d) Elastomeric spline inserts



(e) Wedge splines

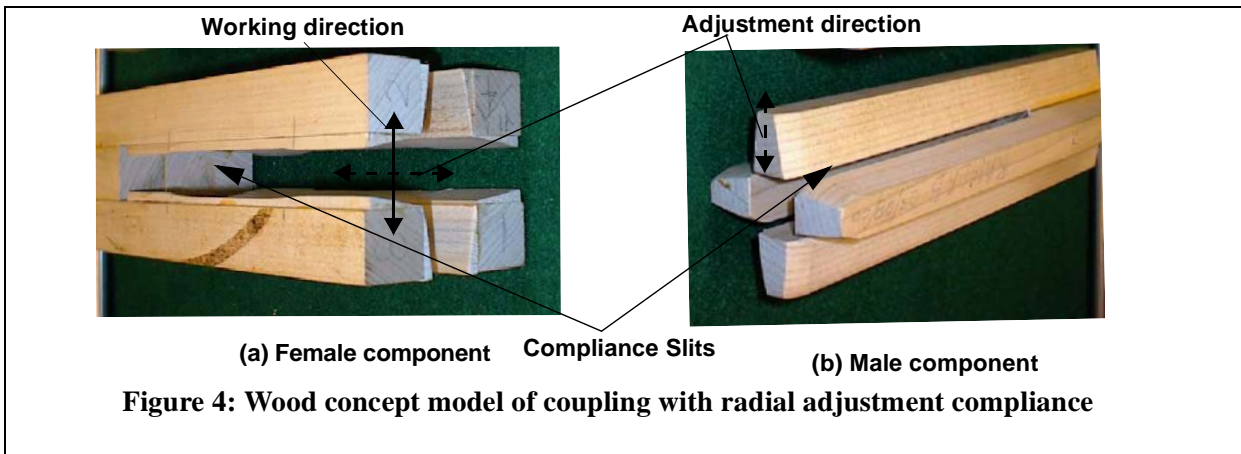
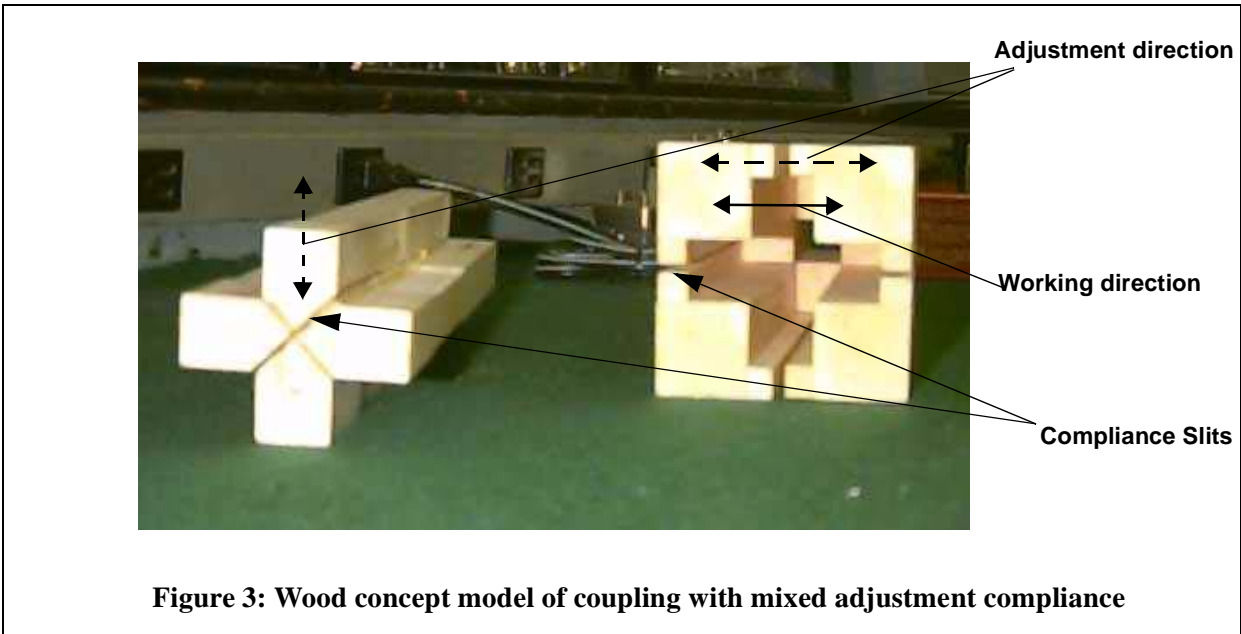
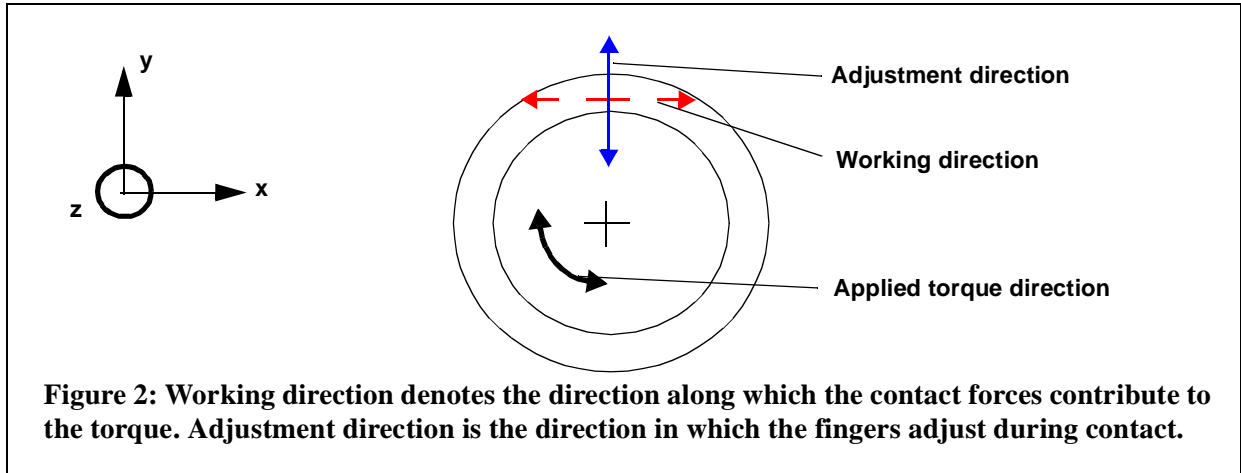


(f) Friction coupling



(g) Self adjusting compliant splines

Figure 1: Conceptual hardware verification





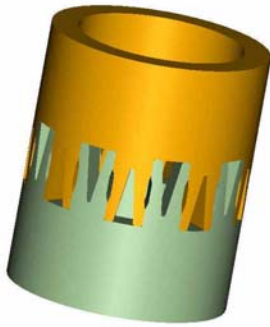
(a) Female component



(b) Male component

Compliance Slits

Figure 5: Wood concept model of coupling with circumferential adjustment compliance and with contact faces being independent

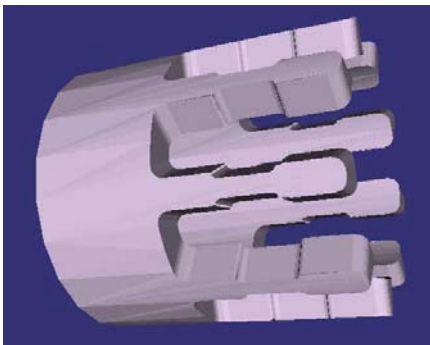


(a) 3-D model of the assembled coupling



(b) 3-D printed part

Figure 6: Non-moment carrying coupling with circumferential adjustment compliance

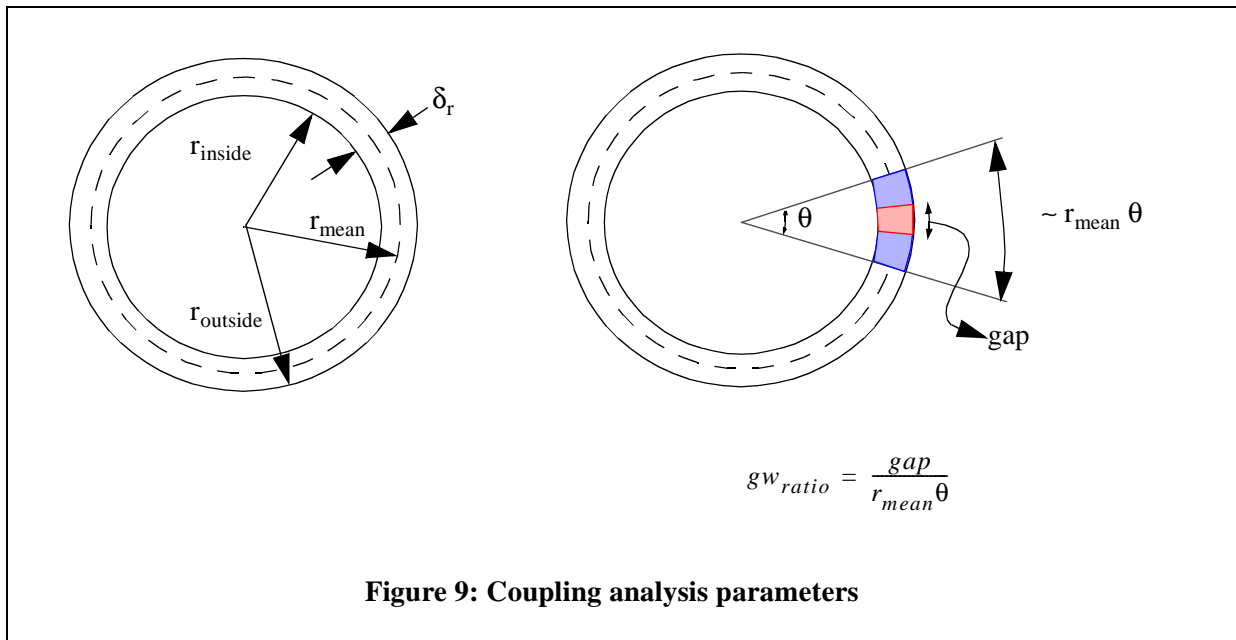
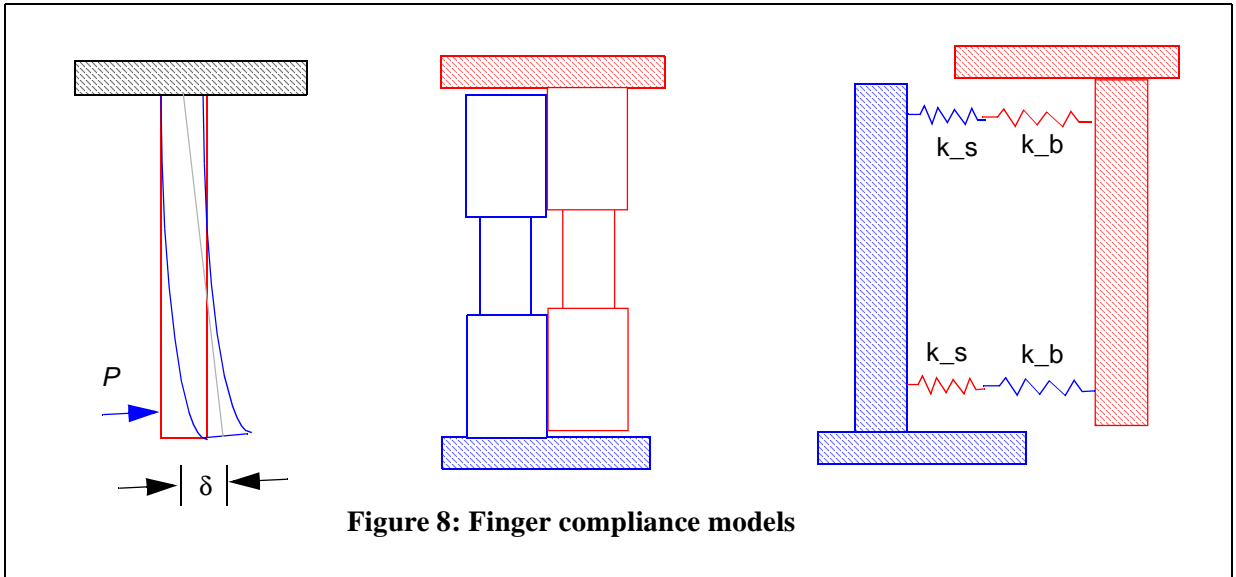


(a) 3-D model of the assembled coupling



(b) 3-D printed part

Figure 7: Non-moment carrying coupling with radial adjustment compliance



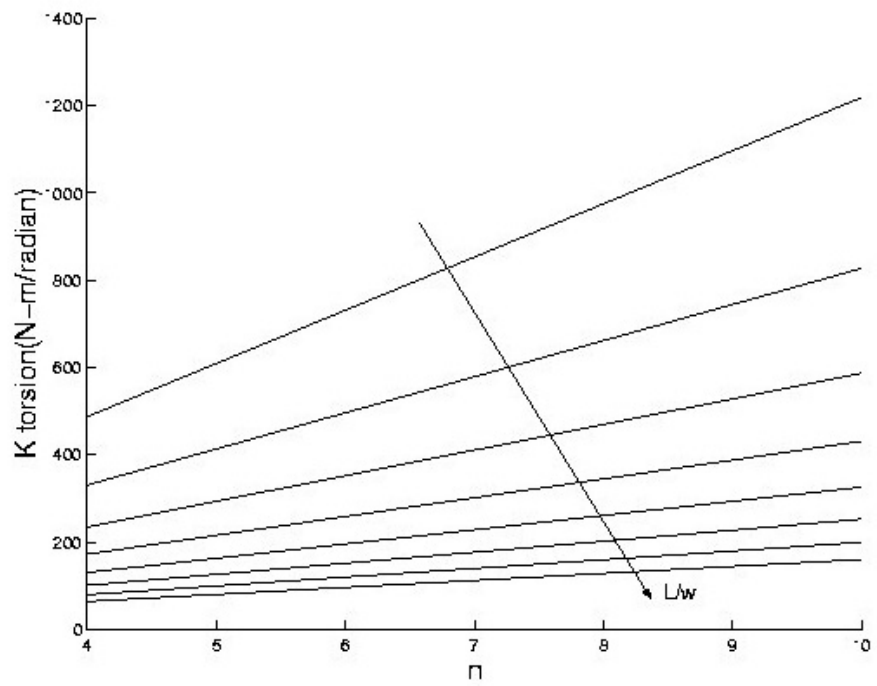
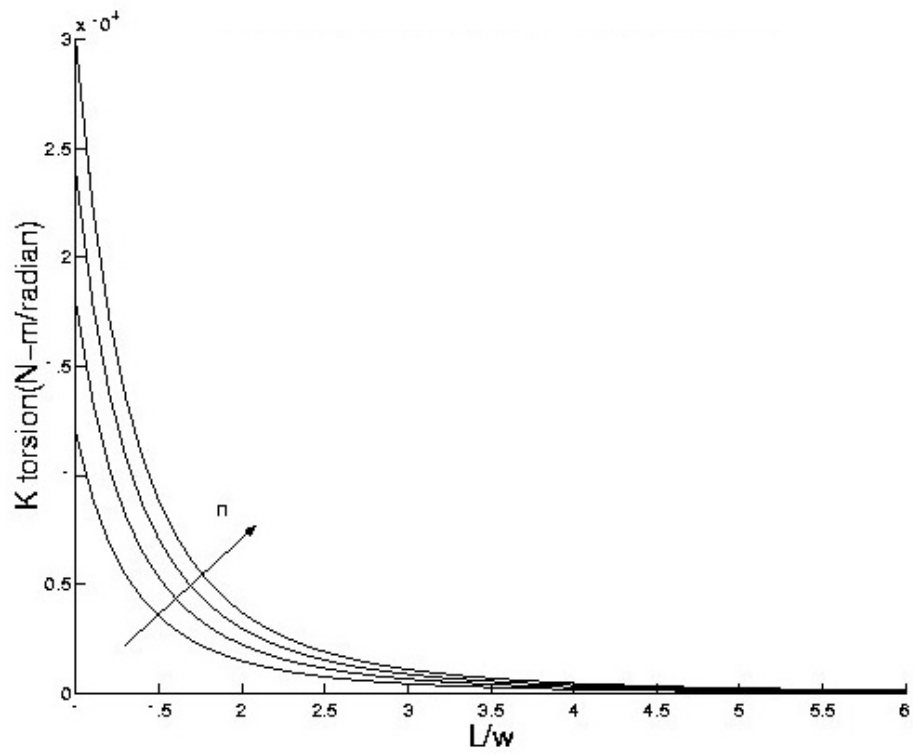


Figure 10: Torsional stiffness variation for circumferential adjustment compliance couplings

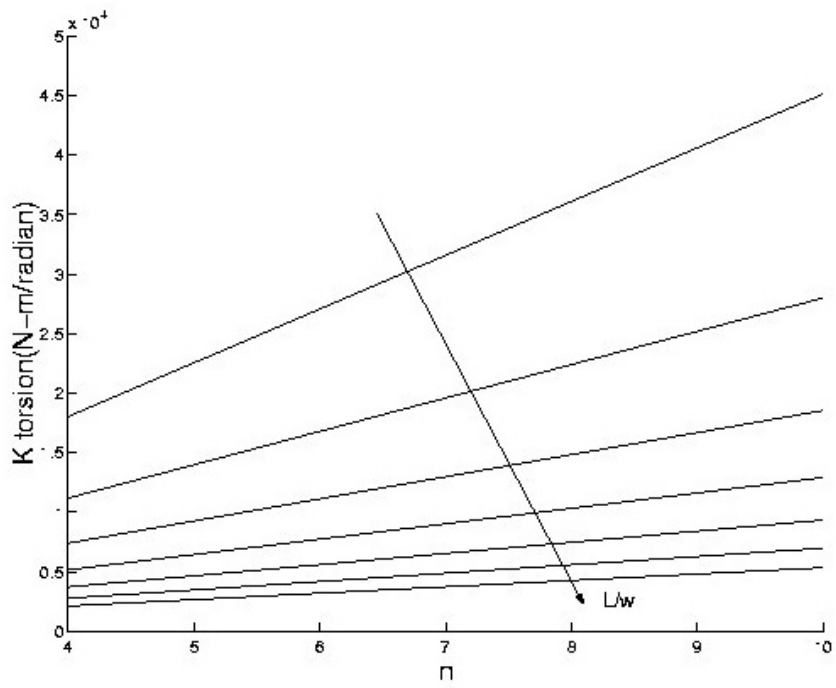
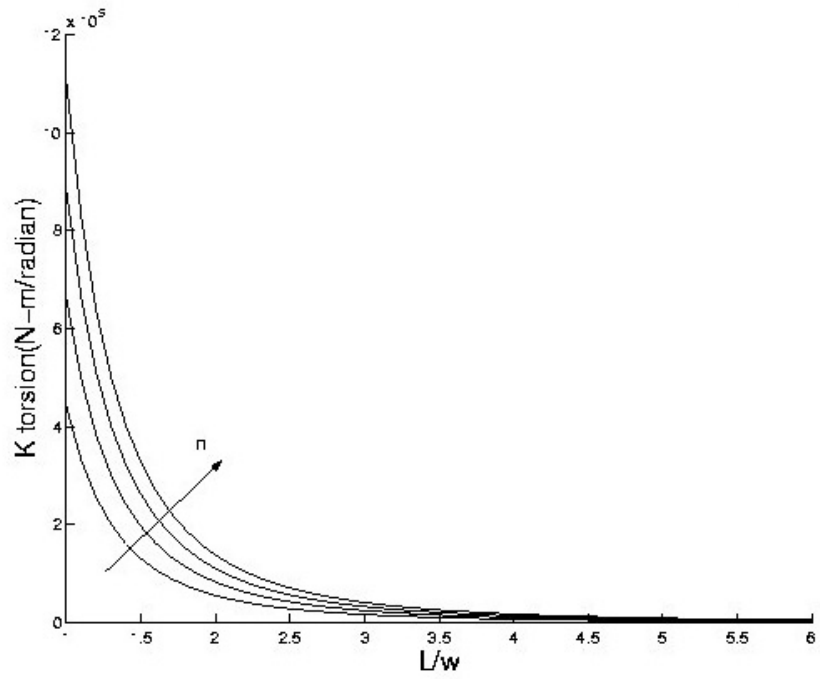


Figure 11: Torsional stiffness variation for radial adjustment compliance couplings

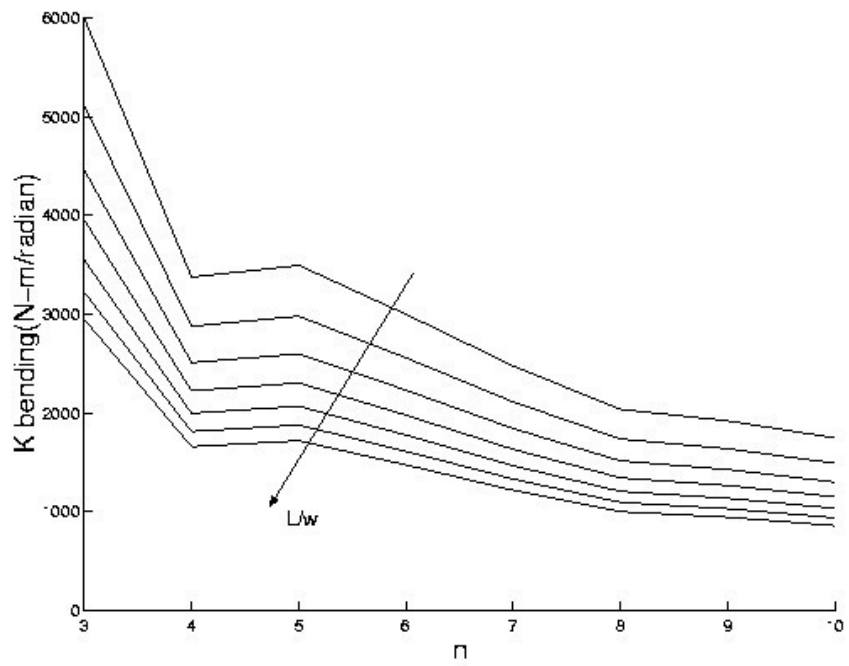
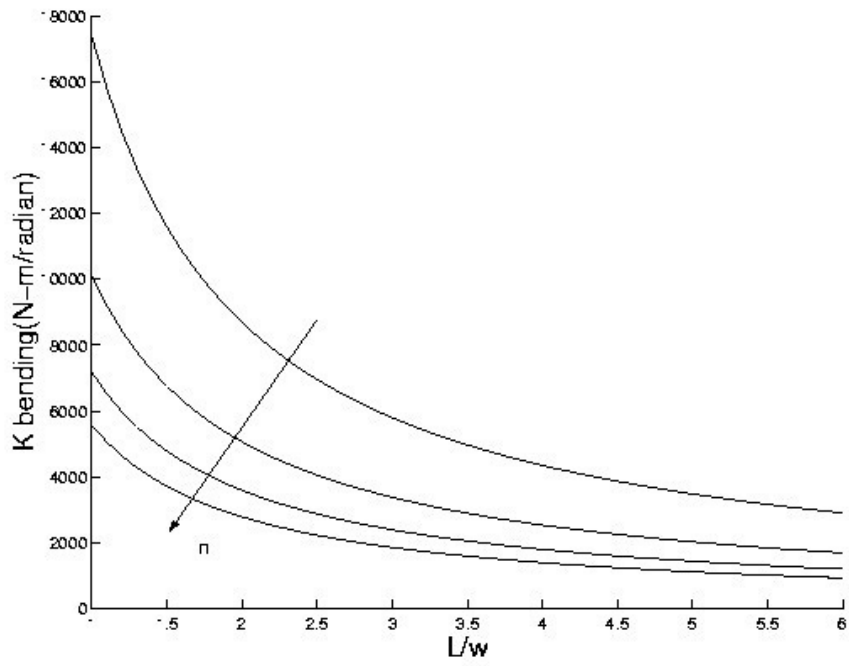


Figure 12: Bending stiffness variation for circumferential adjustment compliance coupling

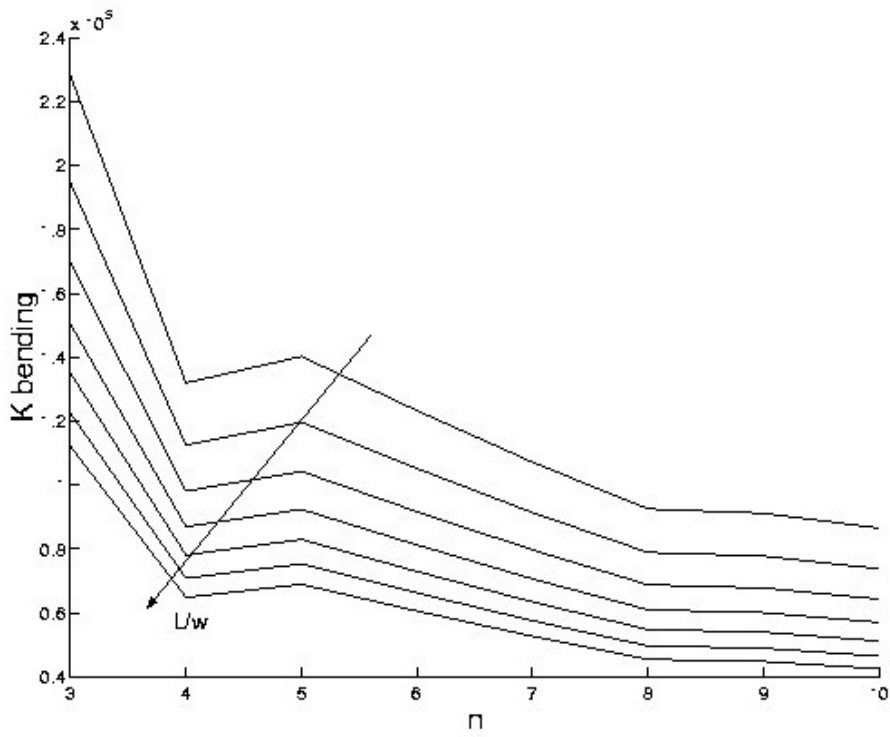
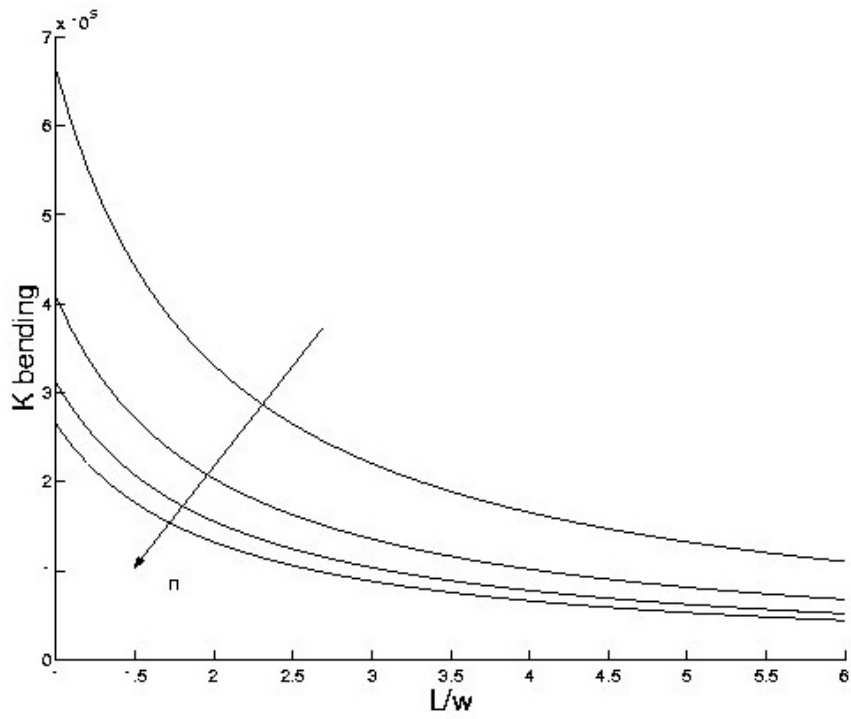
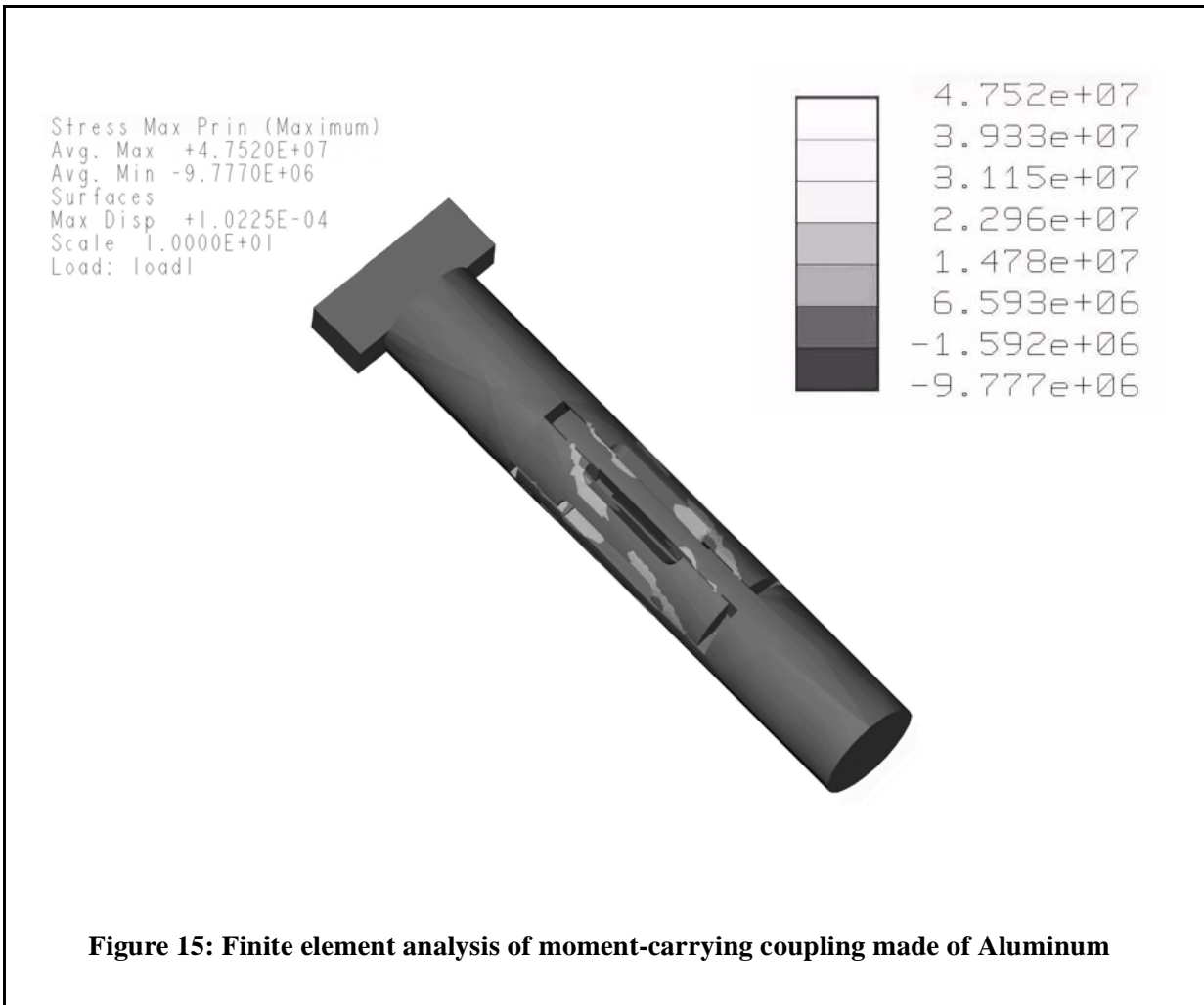
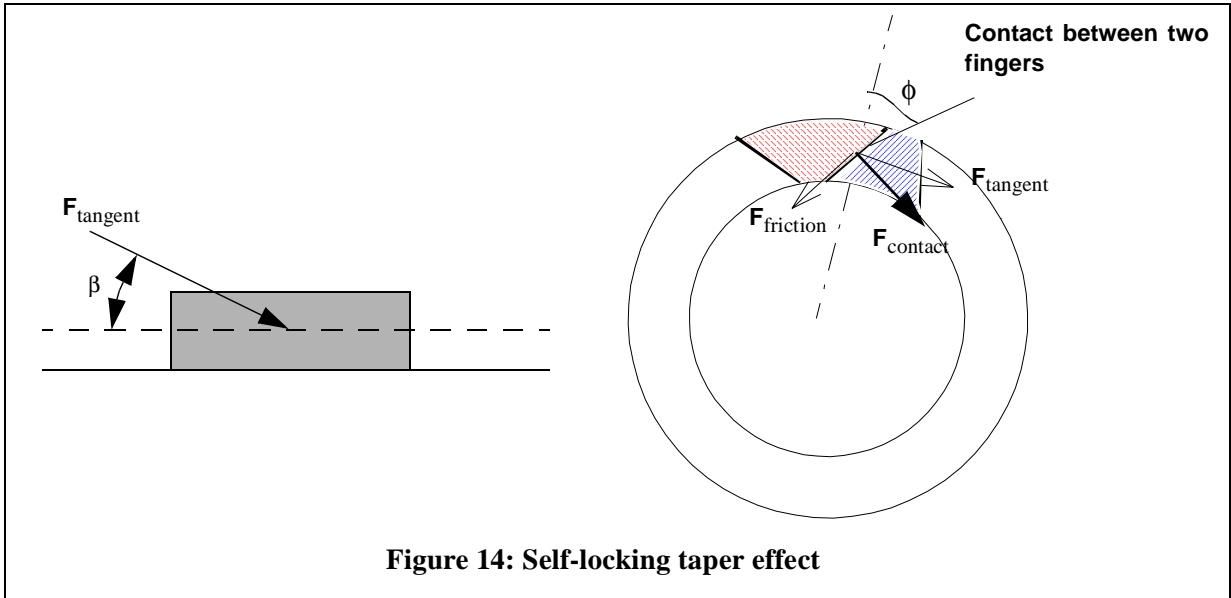
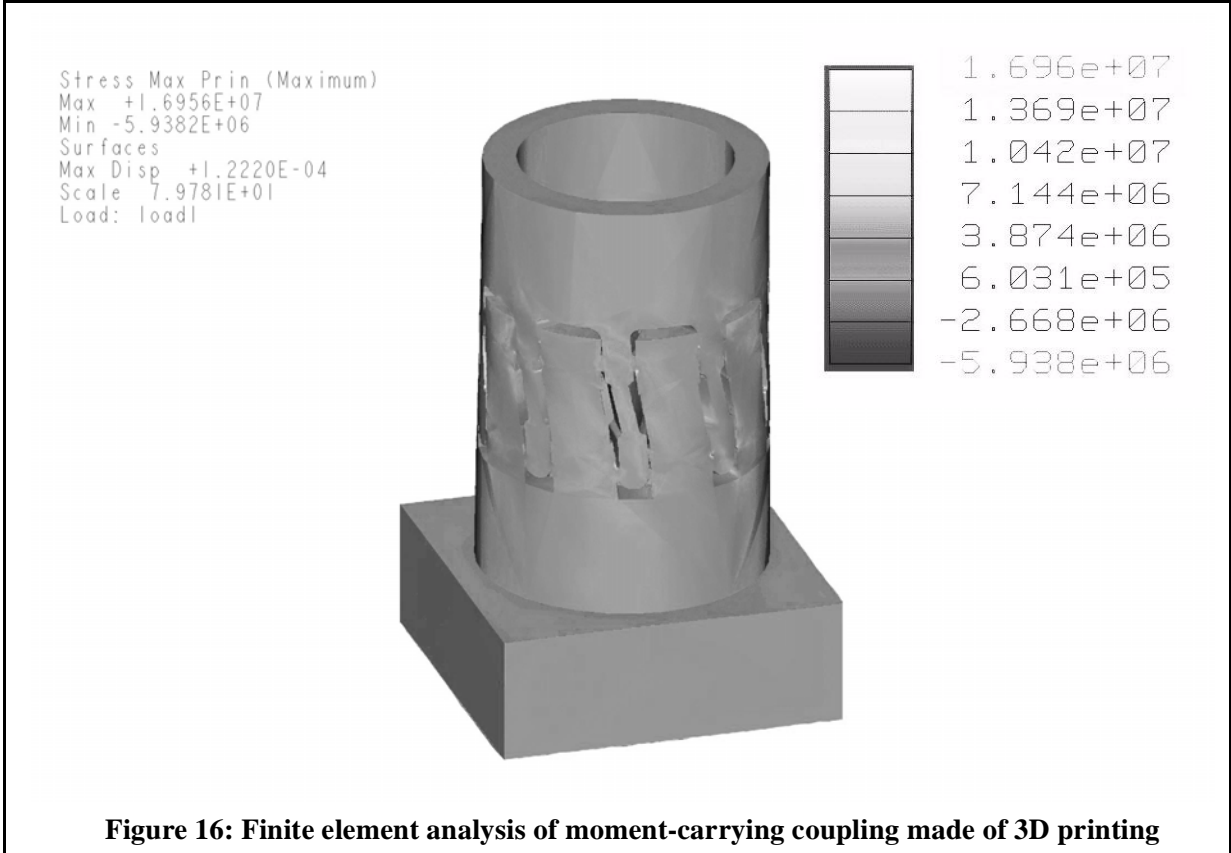
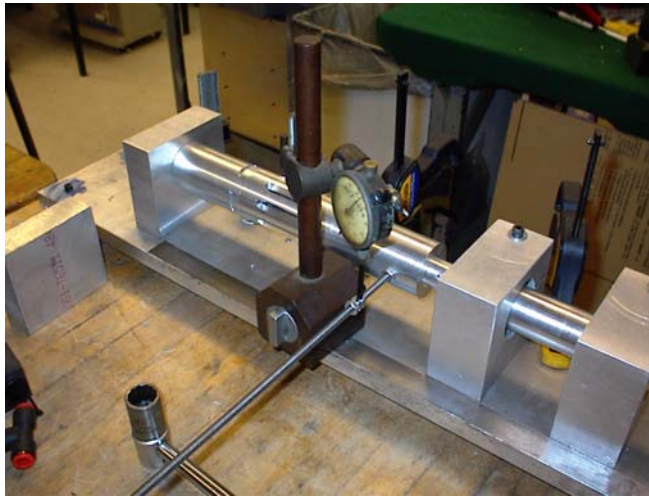


Figure 13: Bending stiffness variation for radial adjustment compliance couplings



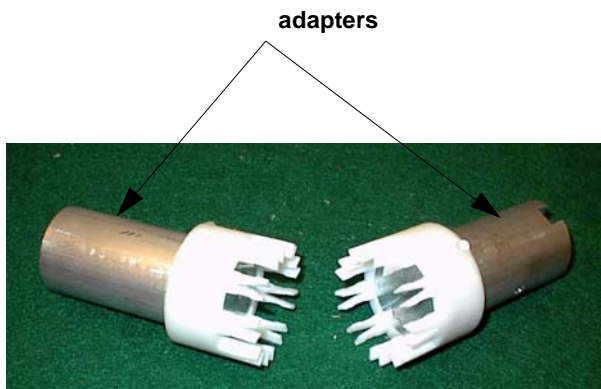




(a) Test Fixture loaded with the aluminum coupling



(b) Aluminum coupling machined from bar-stock



(c) Parallel adjustment 3-D printed coupling with adapters for the test setup



(d) Perpendicular adjustment 3-D printed coupling with adapters for the test setup

Figure 17: Experimental setup for measuring torsional stiffness

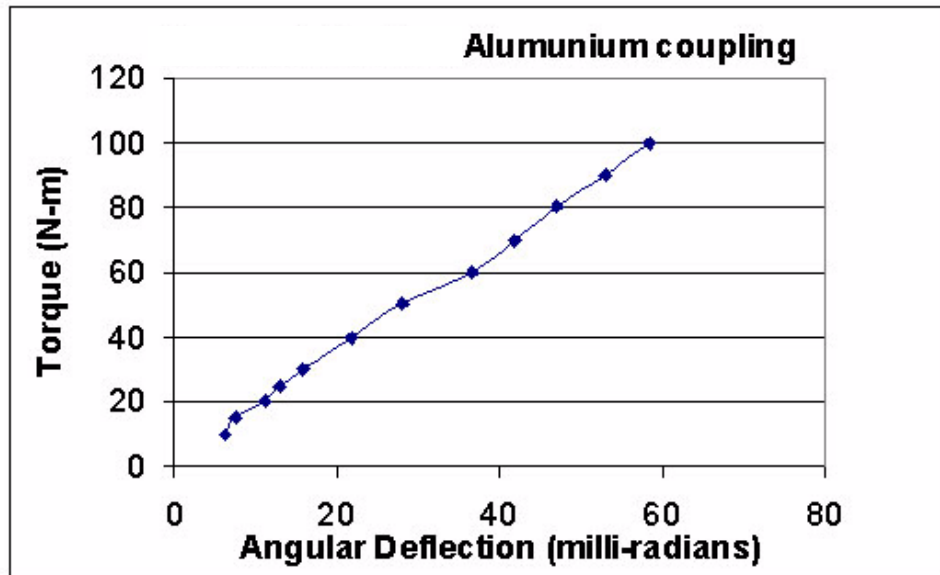
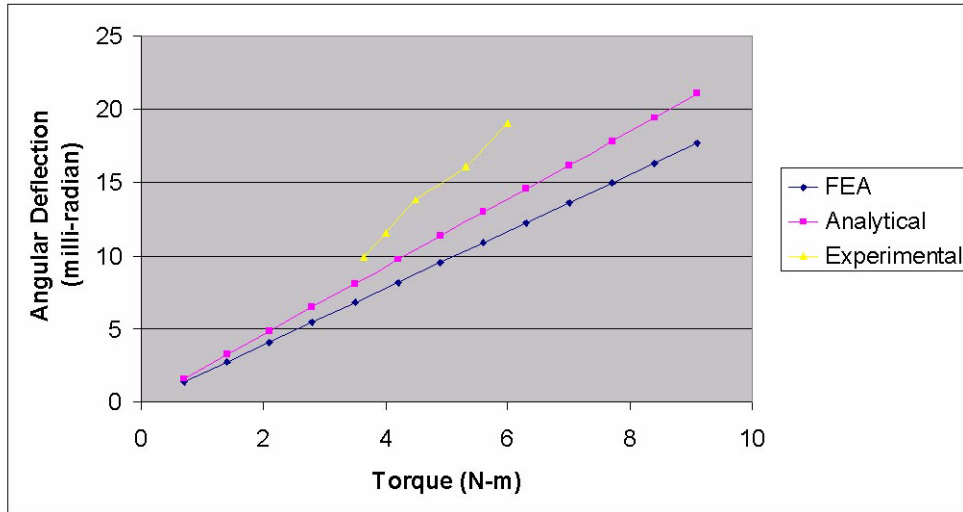
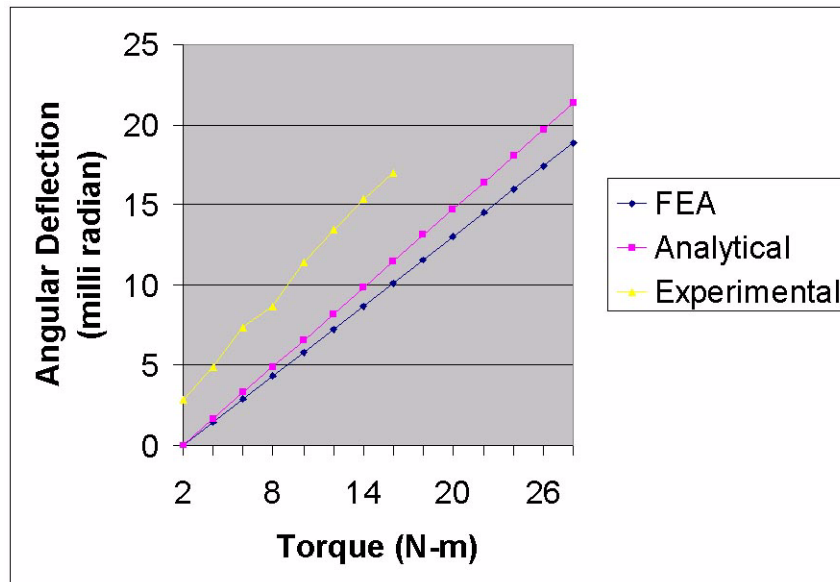


Figure 18: Experimental torsional stiffness for radial adjustment Aluminum coupling concept

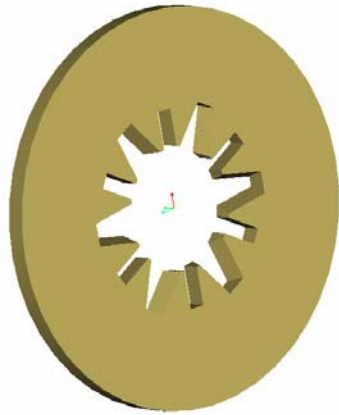


(a) Parallel adjustment 3D printed coupling

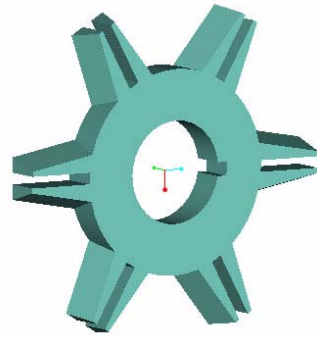


(b) Perpendicular adjustment 3D printed coupling

Figure 19: Experimental torque deflection for 3D printed coupling



(a) Female component



(b) Male component

Figure 20: Radial Coupling concept with self-locking axially tapered adjustment compliance